Journal of Inorganic Biochemistry 250 (2024) 112398

Contents lists available at ScienceDirect

Journal of Inorganic Biochemistry

journal homepage: www.elsevier.com/locate/jinorgbio

Kinetic and structural details of urease inactivation by thiuram disulphides

Luca Mazzei [a,*], Arundhati Paul [a], Michele Cianci [b], Marta Devodier [c,d], Davide Mandelli [c], Paolo Carloni [c,e], Stefano Ciurli [a]

[a] Laboratory of Bioinorganic Chemistry, Department of Pharmacy and Biotechnology (FaBiT), University of Bologna, Viale Giuseppe Fanin 40, Bologna I-40127, Italy
[b] Department of Agricultural, Food and Environmental Sciences, Polytechnic University of Marche, Via Brecce Bianche 10, Ancona I-60131, Italy
[c] Computational Biomedicine, Institute of Advanced Simulations IAS-5/Institute for Neuroscience and Medicine INM-9, Forschungszentrum Jülich GmbH, Jülich D-52428, Germany
[d] Università degli Studi di Parma, Via Università 12, Parma I-43121, Italy
[e] Department of Physics and Universitätsklinikum, RWTH Aachen University, Aachen D-52074, Germany

ARTICLE INFO

Keywords:
Urease
Nickel
Thiuram disulphides
Protein X-ray crystallography
Enzyme inactivation
Quantum mechanical calculations

ABSTRACT

This paper reports on the molecular details of the reactivity of urease, a nickel-dependent enzyme that catalyses the last step of organic nitrogen mineralization, with thiuram disulphides, a class of molecules known to inactivate the enzyme with high efficacy but for which the mechanism of action had not been yet established. IC_{50} values of tetramethylthiuram disulphide (TMTD or Thiram) and tetraethylthiuram disulphide (TETD or Disulfiram) in the low micromolar range were determined for plant and bacterial ureases. The X-ray crystal structure of *Sporosarcina pasteurii* urease inactivated by Thiram, determined at 1.68 Å resolution, revealed the presence of a covalent modification of the catalytically essential cysteine residue. This is located on the flexible flap that modulates the size of the active site channel and cavity. Formation of a Cys-S-S-C(*S*)-N$(CH_3)_2$ functionality responsible for enzyme inactivation was observed. Quantum-mechanical calculations carried out to rationalise the large reactivity of the active site cysteine support the view that a conserved histidine residue, adjacent to the cysteine in the active site flap, modulates the charge and electron density along the thiol S—H bond by shifting electrons towards the sulphur atom and rendering the thiol proton more reactive. We speculate that this proton could be transferred to the nickel-coordinated urea amide group to yield a molecule of ammonia from the generated C_{urea}-NH_3^+ functionality during catalysis.

1. Introduction

The modulation of the enzymatic activity of urease (urea amidohydrolase, EC 3.5.1.5), a nickel-dependent hydrolase that catalyses the breakdown of urea in the last step of organic nitrogen (N) mineralization [1,2], is a crucial goal for agro-environmental sustainability [3–5] and human health [6,7]. The hydrolysis of urea by urease, the most efficient enzyme known [8], causes an increase in the pH of the medium, which in turn is the principal cause of the impact of this process for the release of ammonia in the atmosphere following fertilization of agricultural soils with urea, the most widely used source of nitrogen for crop plants worldwide [9]. Because of this process, it has been estimated that as much as 50% of nitrogen fertilizer applied to soil is not used by crops, a phenomenon that represents a significant economic and environmental cost. Ammonia is a greenhouse gas [10] and further contributes to the formation of particulate matter upon combination with nitrogen and sulphur oxides released upon burning of natural gas and oil in industrial and urban settings [11]. Clearly, there is the need to improve N management to make nitrogen fertilization and crop productivity sustainable [12,13] through the development of efficient urease inhibitors [14].

In addition to the impact of urease in the agro-environmental sector, urease activity of human bacterial and fungal pathogens is used to colonize the host taking advantage of the pH increase in the infected

Abbreviations: TMTD, tetramethylthiuram disulphide; TETD, tetraethylthiuram disulphide; TIPTD, tetraisopropylthiuram disulphide; EC, enzyme classification; AMO, ammonia monooxygenase; JBU, jack bean (*Canavalia ensiformis*) urease; SPU, *Sporosarcina pasteurii* urease; HEPES, (4-(2-hydroxyethyl)-1-piperazineethanesulphonic acid); DMSO, dimethyl sulphoxide; CR, cresol red; MWCO, molecular weight cut-off; EDTA, ethylene diamino tetraacetic acid; MLWF, Maximally Localized Wannier Functions; PDB, protein data bank.

* Corresponding author.
E-mail address: luca.mazzei2@unibo.it (L. Mazzei).

https://doi.org/10.1016/j.jinorgbio.2023.112398
Received 8 August 2023; Received in revised form 21 September 2023; Accepted 7 October 2023
Available online 10 October 2023

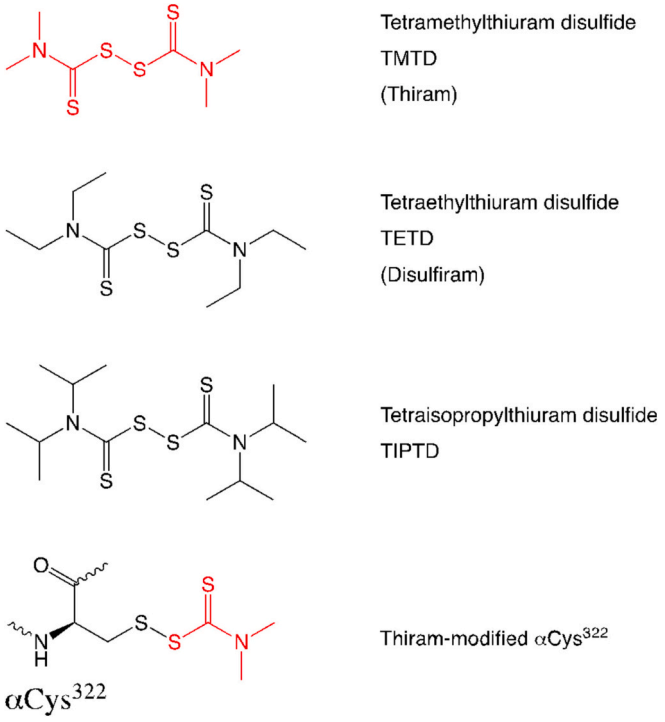

Scheme 1.

milieu [15–17]. *Helicobacter pylori* [18–23], *Staphylococcus aureus* [24], *Mycobacterium tuberculosis* [25–27], as well as *Proteus mirabilis*, *Staphylococcus saprophyticus* as well as a few strains of *Escherichia coli* [28] represent the best-known example of these kind of pathogens. Owing to their crucial role in bacterial survival, ureases have thus become important therapeutic targets for the treatment of diseases caused by urease-dependent pathogenic microorganisms. The World Health Organization has provided a priority list of bacterial [29] and fungal [30] pathogens, the large majority of which use urease activity as a virulence factor.

The development of molecules able to modulate urease activity is a crucial goal for both ecology, agriculture, and public health. Recently, three molecules of the thiuram disulphides family, namely tetramethylthiuram disulphide (TMTD, also known as Thiram), tetraethylthiuram disulphide (TETD, also known as Disulfiram), and tetraisopropylthiuram disulphide (TIPTD) have been reported to reduce urease activity with high efficacy (Scheme 1) [31]. In particular, the activity of jack bean (*Canavalia ensiformis*) urease (JBU), an α_6 hexamer, was observed to decrease by *ca.* 90% and 80% at pH 7.5 upon one-hour incubation of the enzyme with 50 μM of TMTD and TETD, respectively, while TIPTD was significantly less efficient with only 60% activity reduction. The three molecules also drastically decreased the activity of ammonia monooxygenase (AMO) in a culture of *Nitrosomonas europaea*, suggesting their use as potential enhancers of soil nitrogen fertilization that would concomitantly target the two most critical enzymes for the sustainable use of urea as organic fertilizer, namely urease and AMO [31]. However, the fact that Disulfiram has been used as a drug for the treatment of chronic alcoholism [32], and has been studied as a possible treatment for cancer [33] suggests its use also for the treatment of infection by antibiotic-resistant ureolytic bacteria [34]. Recently, the use of Disulfiram has been also associated with a lower risk of COVID-19 infection [35].

While a report was published of Disulfiram inhibiting *Citrullus vulgaris* urease *via* a non-competitive mechanism [36], the general chemical mechanism by which thiuram disulphides affect the activity of urease has not been elucidated, and this is the focus of the present study. Here, we report the measured IC_{50} values of the two most efficient thiurams derivatives, TMTD and TETD, for JBU and *Sporosarcina pasteurii* urease (SPU, an $(\alpha\beta\gamma)_3$ trimer of heterotrimers). In all cases, IC_{50} falls in the low μM range, confirming the high efficacy of thiuram disulphides in decreasing urease activity. The molecular details of the chemical modifications occurring on SPU as a result of its exposure to TMTD were characterized using X-ray crystallography. The refined crystal structure, determined at 1.68 Å, reveals the selective formation

Table 1
X-ray diffraction data collection, processing, and refinement statistics.

Data collection	8Q2E
Wavelength (Å)	0.9797
Detector	PILATUS
Crystal-to-Detector distance (mm)	268.09
Oscillation angle (degrees)	0.100
Number of images	1800
Space group	$P6_322$
Unit cell (*a, b, c,* Å)	131.5, 131.5, 189.0
Resolution range (Å)[a]	1.68–113.89 (1.68–1.71)
Total number of reflections[a]	2,162,471 (109077)
Unique reflections[a]	109,674 (5354)
Multiplicity[a]	19.7 (20.4)
Completeness[a] (%)	100.0 (100.0)
R_{sym}[a,b] (%)	13.6 (240.2)
R_{pim}[a,c] (%)	4.4 (77.6)
Mean I half-set correlation CC(1/2)[a]	0.999 (0.738)
Mean I/σ(I)[a]	18.9 (1.6)
Number of monomers in the asymmetric unit	3
R_{factor}[d] (%)	14.0
R_{free}[d] (%)	16.4
Cruickshank's DPI for coordinate error[e] based on R_{factor} (Å)	0.073
Wilson plot B-factor (Å^2)	21.3
Average all atom B-factor[f] (Å^2)	29.2
B-factor[f] for the Ni atoms (Å^2)	25.2, 24.0
RMS (bonds)[d]	0.013
RMS (angles)[d]	1.814
Total number of atoms	7024
Total number of water molecules	554
Solvent content (%)	54.87
Matthews coefficient (Å^3/Da)	2.72
Favoured regions (%)[g]	90.5
Additional allowed regions (%)[g]	8.4
Generously allowed regions (%)[g]	0.9
Disallowed regions (%)[g]	0.2

[a] Highest resolution bin in parentheses.

[b] $R_{sym} = \sum_{hkl}\sum_j |I_{hkl,j} - \langle I_{hkl}\rangle| / \sum_{hkl}\sum_j I_{hkl,j}$ where $I_{hkl,j}$ is the intensity of a *hkl* reflection, and $\langle I_{hkl}\rangle$ is the mean intensity of all symmetry related reflections j;

[c] $R_{pym} = \sum_{hkl}\sqrt{\frac{1}{n-1}}\sum_{j=1}^{n} |I_{hkl,j} - \langle I_{hkl}\rangle| / \sum_{hkl}\sum_j I_{hkl,j}$ where $I_{hkl,j}$ is the intensity of a *hkl* reflection, and $\langle I_{hkl}\rangle$ is the mean intensity of all symmetry related reflections j, and N is the multiplicity [70];

[d] Taken from REFMAC [46]; R_{free} is calculated using 5% of the total reflections that were randomly selected and excluded from refinement;

[e] $DPI = R_{factor} \bullet D_{max} \bullet compl^{-1/3} \sqrt{\frac{N_{atoms}}{(N_{refl} - N_{params})}}$, where N_{atoms} is the number of the atoms included in the refinement, N_{refl} is the number of the reflections included in the refinement, D_{max} is the maximum resolution of reflections included in the refinement, *compl* is the completeness of the observed data, and for isotropic refinement, $N_{params} \approx 4N_{atoms}$ [71];

[f] Taken from BAVERAGE [70];

[g] Taken from PROCHECK [70].

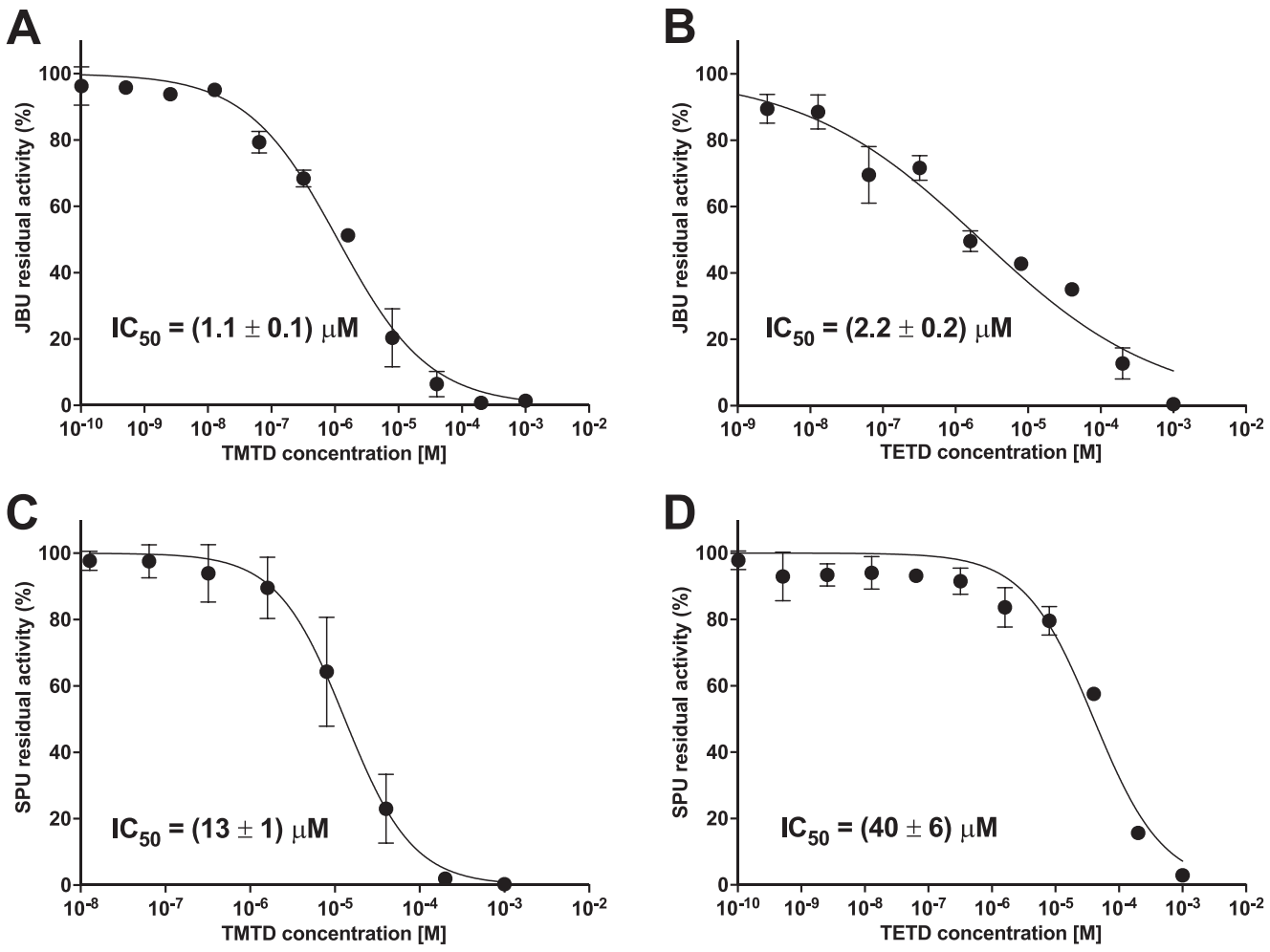

Fig. 1. Dose–response semi-log plot for the residual activity of JBU (A and B) and SPU (C and D) as a function of thiuram disulphide compounds concentration. Experimental data and corresponding non-linear data fitting are shown as dots and lines, respectively. IC_{50} values for each thiuram disulphide compound tested are also reported.

of a αCys^{322}-S-S-C(*S*)-NMe_2 derivative responsible for the irreversible inactivation of the enzyme (Scheme 1). Finally, a rationalization for the differential reactivity of the three different cysteine residues in SPU, also previously observed in multiple cases of urease inactivators, was provided by quantum mechanical calculations that indicated how the presence of αHis^{323}, immediately adjacent to the reactive αCys^{322}, confers a higher acidity to the thiol group, rendering it more reactive.

2. Materials and methods

2.1. Reagents and enzyme preparation

Tetramethylthiuram disulphide (TMTD), tetraethylthiuram disulphide (TETD), and tetraisopropylthiuram disulphide (TIPTD) were purchased from Merck (Milan, Italy). SPU (molar mass = 250 kDa) was purified from *Sporosarcina pasteurii* DSM 33 bacterial cells as previously reported [37]. The active protein was concentrated up to 11 mg mL^{-1} and stored at +4 °C in 50 mM HEPES buffer, 150 mM NaCl, 50 mM Na_2SO_3 and 2 mM EDTA, at pH 7.5. JBU (molar mass = 550 kDa) type C-3, powder (≥ 600,000 units/g) was purchased from Merck (Milan, Italy), dissolved at a final concentration of 50 μg mL^{-1} of active protein in 20 mM HEPES buffer, at pH 7.5, and stored at −80 °C as stock aliquots. Activity quantification of both the enzymes was carried out using the pH-STAT method [38,39] by considering specific activities of 2.5 and 3.5 U $μg^{-1}$ for SPU and JBU, respectively [40].

2.2. IC_{50} measurements

Stock solutions of 10 mM TMTD and TETD were prepared in pure DMSO and used to obtain ten 100-μL serial dilutions in the 5 μM – 10 mM range, using the same solvent. Subsequently, 900 μL of CR buffer (30 mg L^{-1} of cresol red dissolved in 2 mM HEPES buffer, at pH 7.5, also including 2 mM EDTA), containing 0.5 μg mL^{-1} of active JBU or SPU, was added to each previously prepared thiuram disulphide aliquot, thus obtaining incubation mixtures of enzyme and inhibitor in the 0.5 μM – 1 mM range in CR buffer, and 10% DMSO. After a one-hour incubation, aimed at reaching the equilibrium between the enzyme and each thiuram disulphide, the enzymatic reaction was started by the addition of 12.5 μL of a 8 M urea solution, reaching a final concentration of 100 mM. A spectrophotometric assay, performed using an Agilent Cary 60 UV − Vis spectrophotometer, was carried out by following the change in absorbance at 573 nm due to the pH-dependent change in the colour of

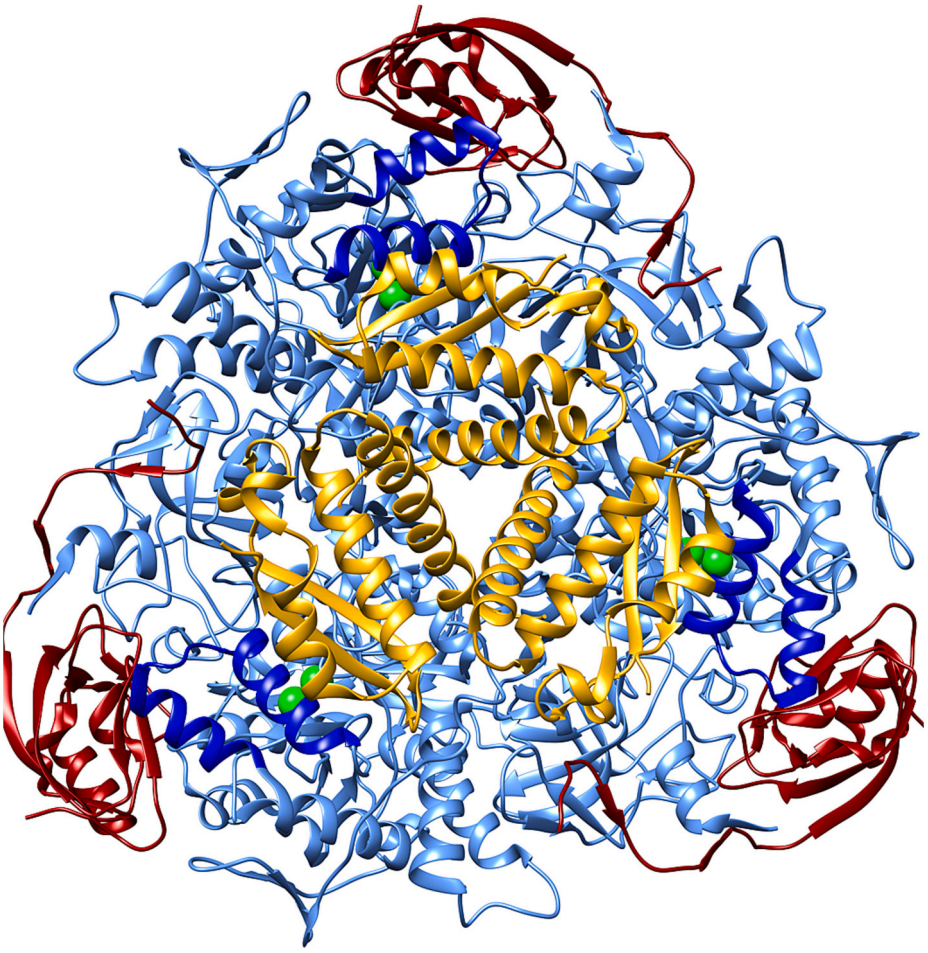

Fig. 2. Ribbon scheme of native SPU; chain α, β, and γ of each trimer is coloured cornflower blue, dark red, and gold, respectively. The Ni(II) ions in the active sites of each trimer are shown as green spheres, while the mobile flap regions covering the active site cavities (residues 310–340 of each α chain) are coloured dark blue. Figure made with UCSF Chimera 1.15 [72]. (For interpretation of the references to colour in this figure legend, the reader is referred to the web version of this article.)

cresol red, and monitored over time. The experiments were conducted in triplicates for each concentration of TMTD or TETD. The initial reaction rate (v_i) was calculated as the slope of the linear portion of the absorbance *vs.* time curve. The resulting values for each set of samples were averaged, normalized with respect to the initial reaction rate in the absence of either thiuram disulphide (v_0), and the obtained percentage residual activity values were plotted as a function of the inhibitor concentration on a semi-log graph. The inhibitor concentration values leading to a 50% inactivation of the enzyme (IC_{50}) were then estimated by fitting the resulting data with the canonical dose – response curve for the calculation of the IC_{50} values in the Prism v. 8.4.3 software.

2.3. Crystallization, data collection and structural determination

A 11 mg mL^{-1} aliquot of SPU was buffer-exchanged, through successive dilution – concentration cycles using Amicon Ultra centrifugal filter units - MWCO 10 KDa (Merck), in 50 mM HEPES buffer, 150 mM NaCl, and 2 mM EDTA, at pH 7.5, to decrease Na_2SO_3 concentration down to *ca.* 20 μM. A clear stock solution of 17 mM TMTD was prepared in pure DMSO and added 1:10 (*v*/v) to the buffer-exchanged SPU solution, thus obtaining an incubation mixture of 10 mg mL^{-1} SPU (40 μM $(\alpha\beta\gamma)_3$ trimer of heterotrimers, 120 μM (αβγ) biological unit) and 1.7 mM TMTD in the crystallization buffer, also containing 10% (v/v) DMSO. After *ca.* three hours of incubation, during which the enzyme activity was abolished (checked using a colorimetric assay based on cresol red), the mixture was used to set up crystallization trials by mixing 1.5 μL of the SPU-TMTD solution with an equal volume of precipitant (1.6–2.1 M $(NH_4)_2SO_4$ dissolved in 50 mM sodium citrate buffer, at pH 6.3) and equilibrating the resulting crystallization drops through vapor diffusion (hanging-drop method) at 293 K against 1 mL of the precipitant solution in 24-well XRL plates (Molecular Dimensions, Suffolk, U.K.). Since TMTD was absent in the precipitant solution, crystallization occurred in the presence of 0.85 mM ligand. Rice-shaped protein crystals (0.05 × 0.05 × 0.1 mm^3) grew at a concentration of 2.0 $(NH_4)_2SO_4$ after two weeks. Crystals were scooped up using LithoLoops cryoloops (Molecular Dimensions, Suffolk, U.K.), transferred to a cryoprotectant solution containing 50 mM citrate buffer at pH 6.3 containing 2.4 M $(NH_4)_2SO_4$, and 20% (*v*/v) ethylene glycol, and then flash-cooled and stored in liquid nitrogen. Crystallization trials of SPU in the presence of TETD were also set up using the same experimental protocol, but no crystals were obtained.

Diffraction data were collected at 100 K using synchrotron X-ray radiation at the EMBL P13 beamline of the Petra III storage ring, c/o DESY, Hamburg (Germany) [41]. Helical data collection was performed

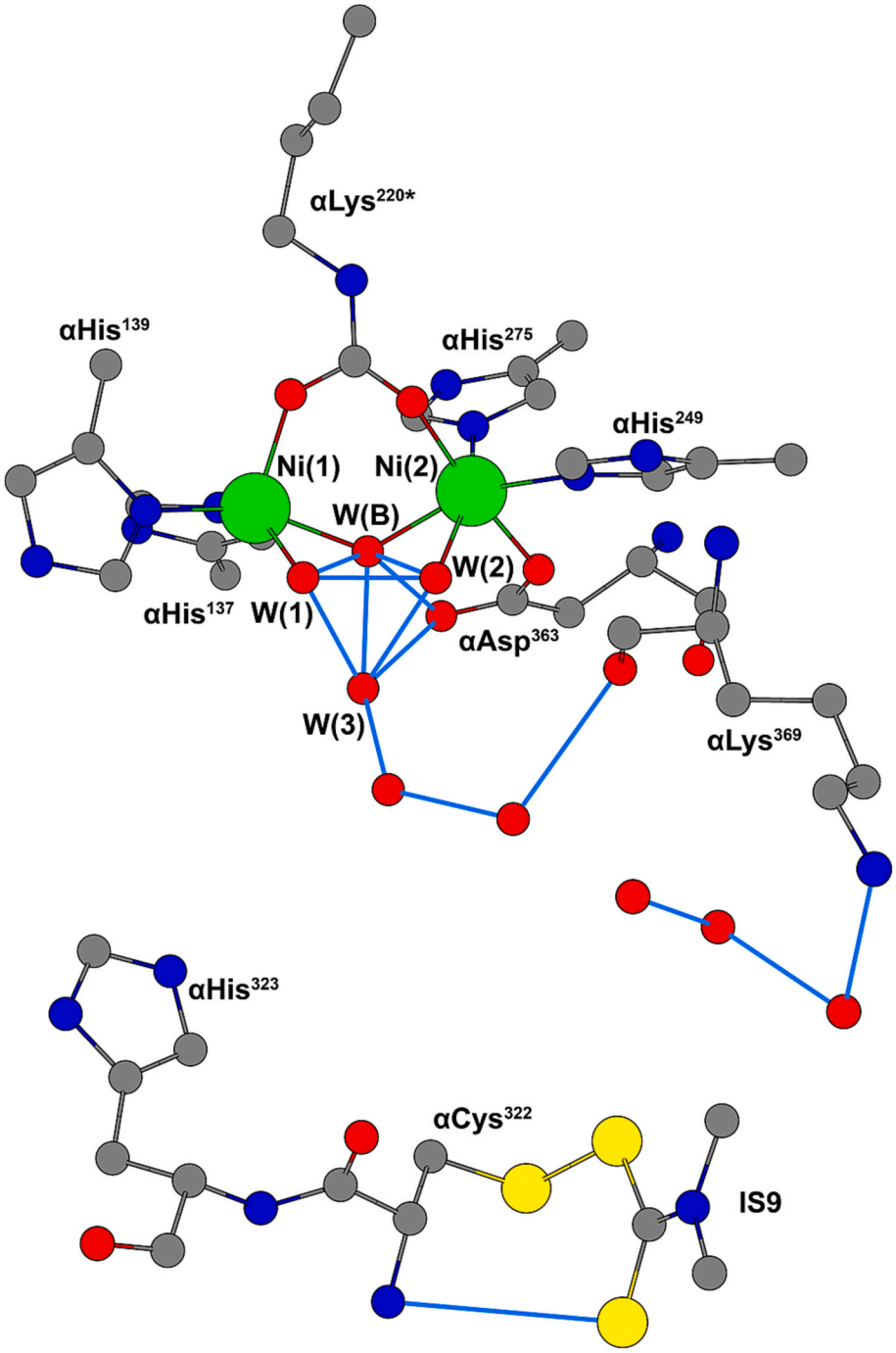

Fig. 3. Crystallographic structural model for the active site obtained for the thiram-inhibited SPU. The carbon, nitrogen, oxygen, sulphur and nickel atoms are grey, blue, red, yellow and green, respectively. Putative H-bonds are shown as blue lines. Spheres are drawn using the relative atomic radii values in CrystalMaker v. 10.7.2. (For interpretation of the references to colour in this figure legend, the reader is referred to the web version of this article.)

to achieve higher data quality by minimizing protein crystal radiation damage. Data processing and reduction were carried out using XDS [42] *and AIMLESS* [43,44]. The X-ray crystal structure of SPU bound to catechol (PDBid 5G4H, 1.50 Å resolution) [45], devoid of solvent molecules and ligands, and after coordinates randomization, was used as a starting model to obtain the initial phases for the structure determination. Restrained refinement was carried out using REFMAC5 [46] and isotropic atomic displacement parameters (ADPs) (including the hydrogen atoms in the riding positions). Manual model rebuilding, as well as water or ligand addition/inspection were conducted using COOT [47,48]. Unbiased omit electron density maps for non-proteinaceous ligands were calculated using Fourier coefficients F_o - F_c and phases from the last cycle of refinement before ligand addition to the refining model. The X-ray crystal structure was determined at a final resolution of 1.68 Å, and the resulting structure factors and atomic coordinates were deposited in the Protein Data Bank with the accession code 8Q2E. Data collection and final refinement statistics are given in Table 1.

2.4. Quantum-mechanical calculations

The αCys^{322}-αHis^{323} (*Cys-His*) and the αCys^{322} (*Cys*) models were built starting from the crystal structure of SPU inhibited by fluoride in

Table 2
Selected distances and angles around the Ni(II) ions in the X-ray crystal structure of SPU incubated in the presence of TMTD and bound to dimethyldithiocarbamate. Values are compared to those reported for the native urease (PDBid 4CEU).

PDBid [a]	8Q2E	4CEU [b]
Ni - L Distances (Å)		
Ni(1) - αLys220* Oθ1	2.0	2.0
Ni(1) - L_B	2.0	1.9
Ni(1) - L_1	2.1	2.2
Ni(1) - αHis249 Nδ	2.0	2.0
Ni(1) - αHis275 Nε	2.0	2.1
Ni(2) - αLys220* Oθ2	2.1	2.1
Ni(2) - L_B	2.1	2.0
Ni(2) - L_2	2.1	2.2
Ni(2) - αHis137 Nε	2.1	2.1
Ni(2) - αHis139 Nε	2.1	2.1
Ni(2) - αAsp363 Oδ1	2.1	2.1
Ni(1) ••• Ni(2)	3.6	3.6
L_1 ••• L_2	2.2	2.3
L - Ni - L Angles (degrees)		
αLys220* Oθ1 - Ni(1) - αHis249 Nδ	102.5	101.3
αLys220* Oθ1 - Ni(1) - αHis275 Nε	104.1	107.2
αLys220* Oθ1 - Ni(1) - L_B	94.4	89.9
αLys220* Oθ1 - Ni(1) - L_1	106.2	107.9
αHis249 Nδ - Ni(1) - αHis275 Nε	96.8	95.3
αHis275 Nε - Ni(1) - L_B	100.1	101.9
L_B - Ni(1) - L_1	62.7	70.1
L_1 - Ni(1) - αHis249 Nδ	91.4	85.8
αHis249 Nδ - Ni(1) - L_B	152.3	155.7
αHis275 Nε - Ni(1) - L_1	146.0	143.9
αLys220* Oθ2 - Ni(2) - αHis137 Nε	94.4	92.1
αLys220* Oθ2 - Ni(2) - αHis139 Nε	92.2	92.6
αLys220* Oθ2 - Ni(2) - L_2	89.8	93.3
αLys220* Oθ2 - Ni(2) - L_B	93.2	90.2
αAsp363 Oδ1 - Ni(2) - αHis137 Nε	80.8	81.6
αAsp363 Oδ1 - Ni(2) - αHis139 Nε	85.5	84.3
αAsp363 Oδ1 - Ni(2) - L_2	96.2	94.5
αAsp363 Oδ1 - Ni(2) - L_B	91.7	96.0
L_2 - Ni(2) – L_B	64.3	69.9
L_B - Ni(2) - αHis137 Nε	95.6	91.7
αHis137 Nε- Ni(2) - αHis139 Nε	111.2	112.2
αHis139 Nε- Ni(2) - L_2	88.3	85.9
αLys220* Oθ2 - Ni(2) - αAsp363 Oδ1	173.5	171.3
L_B - Ni(2) - αHis139 Nε	152.1	155.8
L_2- Ni(2) - αHis137 Nε	159.7	160.8
Ni(1) - L_B - Ni(2)	125.2	135.1

[a] L_1, L_2 indicate the ligand atom bound to Ni(1) and Ni(2), respectively, while L_B indicates the Ni-bridging ligand atom.
[b] Data taken from [60].

complex with the substrate urea (PDBid: 6QDY[11]). Methyl groups replaced the peptide units of αVal^{321} and αHis^{324}. Missing hydrogen atoms were added assuming standard bond lengths and angles using the pdb2gmx tool of the GROMACS suite of codes [49,50]. The thiol proton was located so that its distance from the imidazole ring was as short as possible. Inspection of the X-ray structure suggests that αHis^{323} Nδ atom forms an H-bond with αAsp^{224} Oδ2 and it is therefore considered protonated. αHis^{323} Nε forms an H-bond with αArg^{339} terminal NH_2 group, and is thus considered not protonated, resulting in a neutral state of this residue, as previously discussed in the case of the active site closed flap conformation [51,52].

All calculations were performed *in vacuo* using the density functional theory code CPMD v4.3 [53] at the B3LYP [54] level of theory. Kohn-Sham orbitals were expanded using a plane-wave basis set with a cut-off of 100 Ry. A simulation box of dimensions 15.0 Å × 15.0 Å × 15.0 Å was employed. Isolated system conditions were achieved by using the method of Martyna and Tuckerman [55]. Only valence electrons were considered, using Trouillers-Martins norm conserving pseudopotentials to describe core electrons - valence electrons interactions [56]. Geometry optimization was carried out using CPMD v4.3 with a convergence criterium of 36 meV/Å for geometry and 6.7×10^{-7} Å^{-3} for orbitals.

The Maximally Localized Wannier Functions (MLWF) [57,58] and the electron density (ρ) of the *Cys-His* dimer and the *Cys* monomer models were calculated using CPMD v4.3 [53]. The change in MLWF was quantified by computing the variation of the distance of their centres from the sulphur atom. The change in electronic density was computed as $\Delta\rho = \rho^{Cys\text{-}His} - \rho^{Cys}$. The change in the atomic charge was obtained by integrating Δρ over the Voronoi volume of each atom [59].

3. Results and discussion

In order to ascertain the biochemical aspects of the inactivation of urease by thiuram disulphides, enzymatic reaction rates were measured after one hour of incubation in the presence of increasing concentrations of TMTD, TETD, and TIPTD. The results are presented only for TMTD and TETD, because the assays in the presence of TIPTD returned irreproducible results, probably due to solubility limits of the ligand, and were not further pursued. Semi-log dose-response plots as a function of the inhibitor concentration are shown in Fig. 1. In all cases the experimental data show a nearly sigmoidal profile to reach full enzyme inactivation and were fitted to the canonical equation used to determine IC_{50} values. The IC_{50} values obtained for TMTD and TETD on JBU and SPU (Fig. 1) fall in the low micromolar concentration range, confirming the high efficiency of the enzyme inactivation by these molecules.

In order to depict, at the molecular level, the mode of inhibition of thiuram disulphides on urease, co-crystals of SPU and TMTD were obtained and investigated by single crystal X-ray diffraction. The crystals belong to space group $P6_322$, isomorphous with all the crystal structures of SPU determined so far. The refined structure shows the $(\alpha\beta\gamma)_3$ quaternary assembly typical of SPU (Fig. 2), where the α subunit is formed by an $(\alpha\beta)_8$-barrel domain and a β-type domain, the β subunit is mainly characterized by β strands, and the γ subunit consists of αβ domains. The overall backbone folding of the three protein chains is conserved with respect to the corresponding chains of the enzyme crystallized in the native form (PDBid 4CEU) [60] (Cα RMSD equal to 0.153 Å, 0.136 Å, and 0.100 Å for chains α, β, and γ, respectively).

The architecture of the Ni-containing active site region in the refined X-ray crystal structure, including its hydration environment, is completely conserved with respect to that of the native enzyme (Fig. 3 and Table 2): two well-ordered Ni(II) ions are separated by *ca.* 3.7 Å, and bridged by the Oθ1 and Oθ2 atoms of a carbamylated αLys^{220}* residue and a hydroxide ion W(B). Ni(1) is additionally bound to αHis^{249} Nδ and αHis^{275} Nε, while Ni(2) is bound to αHis^{137} Nδ, to αHis^{139} Nε, and to αAsp^{363} Oδ1. A distorted square-pyramidal and a distorted octahedral coordination for Ni(1) and Ni(2), respectively, are completed by the presence of two well-ordered solvent molecules, namely W(1) and W(2), while an additional W(3) is located in a distal position and at H-bonding distance from W(B), W(1) and W(2).

The analysis of the unbiased omit electron density map of the X-ray crystal structure disclosed an additional unmodelled electron density in the vicinity of the flap and proximal to the αCys^{322} residue (Fig. 4A) that was successfully interpreted by modelling a dimethyldithiocarbamate moiety (defined as IS9) (Fig. 4B) covalently bound to αCys^{322} Sγ through its S atom, with a S—S distance of 2.1 Å (Fig. 3). The final adduct obtained on αCys^{322} suggests the occurrence of a thiol-disulphide exchange reaction between the free thiol of αCys^{322} and the R-S-S-R group of TMTD.

The results of the crystal structure analysis clearly indicate that the enzyme inactivation in the presence of thiuram disulphides does not involve the essential Ni(II) ions in the active site of this metalloenzyme, but rather targets αCys^{322}, known to play a critical role in the catalytic mechanism [61,62]. This residue is located on a helix-loop-helix motif, the "active site flap", that is known to be involved in the catalytic mechanism by regulating the opening of the active site channel and stabilizing the coordination of the substrate urea to the essential Ni(II) ions [8,51]. However, the mode of action of αCys^{322} in the enzymatic

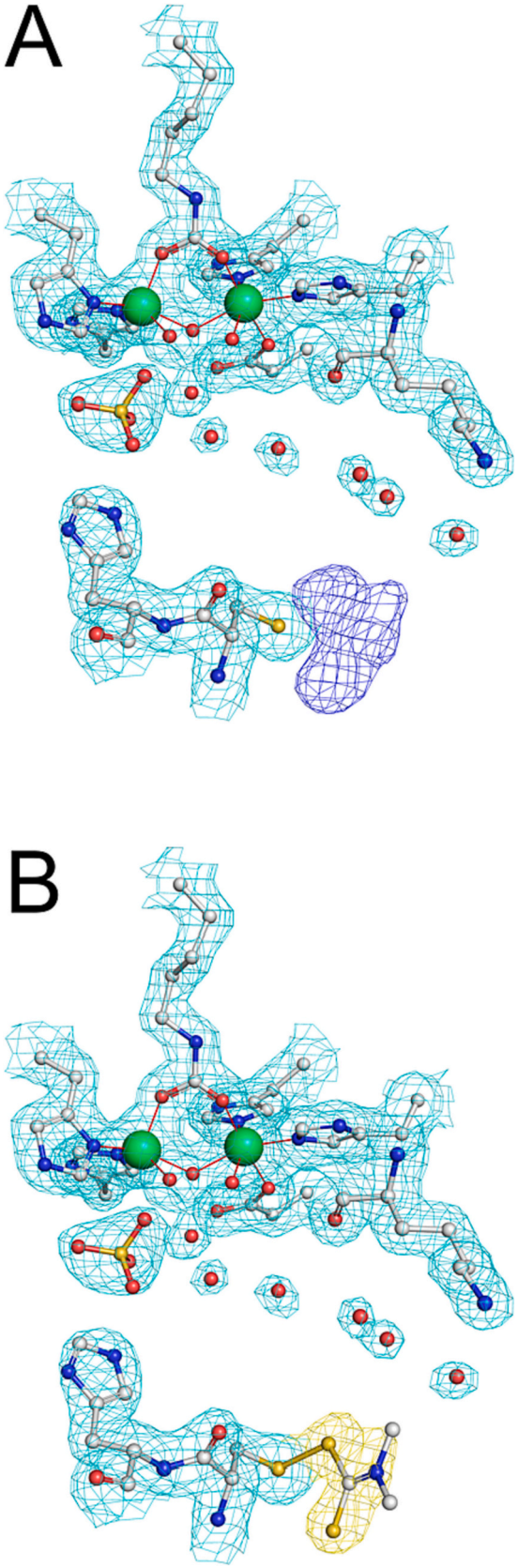

Fig. 4. X-ray crystal structure of SPU incubated in the presence of TMTD and bound to dimethyldithiocarbamate in the active site region. (A) The protein atomic model, as well as the nickel ions and the solvent molecules, are shown superimposed onto the final $2F_o - F_c$ electron density map, contoured at 1σ and coloured grey. The unbiased $F_o - F_c$ omit electron density map for the ligand is shown contoured at 3σ and coloured blue. (B) The same environments are presented showing the modelled thiocarbamate superimposed onto the final $2F_o - F_c$ electron density map, contoured at 1σ and coloured yellow. Carbon, nitrogen, oxygen, sulphur, and nickel are shown in grey, blue, red, yellow, and green, respectively. Figure made with PyMol (The PyMOL Molecular Graphics System, v. 2.4.1, Schrödinger, LLC.). The orientation and labelling is the same as Fig. 3. (For interpretation of the references to colour in this figure legend, the reader is referred to the web version of this article.)

(caption on next column)

catalysis has never been fully clarified. Clues to elucidate the role of this residue in the enzymatic catalysis could be derived from structural evidence collected on SPU inactivated by β-mercaptoethanol (PDBid 1UBP [63]), Ag(I) (PDBid 7B58, 7B59, 7B5A and 6G48 [64,65]), catechol derivatives (PDBid 5G4H, 6ZNY, 6ZNZ, 6ZO0, 6ZO1, 6ZO2, 6ZO3 [45,66]), and Ebselen (PDBid 7ZCY [67]), which highlighted the peculiar reactivity of αCys^{322}, differing from αCys^{555}, the other solvent-exposed cysteine residue present on SPU (a third cysteine residue, αCys^{520}, is located deep in the core of the α chain and is not susceptible to chemical modifications). In particular, in all the cases cited above as well as in the case of TMTD, the chemical modifications of αCys^{322} are not observed for αCys^{555}, indicating a higher reactivity of the cysteine residue on the active site flap. A specific feature of αCys^{322} is the presence, in its immediate surroundings, of the αHis^{323} residue, which is conserved and known to be essential for urease activity [68]. Density functional theory calculations using a plane-wave basis set allowed us to investigate whether and how αHis^{323} could modify the reactivity of αCys^{322}. The polarization of the αCys^{322} S—H bond was investigated in terms of the rearrangements of the Maximally Localized Wannier Functions (MLWF) [57,58] as well as of the electron density of αCys^{322}, as induced by the presence of αHis^{323}. The MLWF are obtained by a unitary transformation of the Kohn-Sham orbitals and they are equivalent to the localized molecular orbitals, or "Boys orbitals" as known in quantum chemistry. The maxima of these functions (Wannier centres) provide a useful representation of chemical concepts such as electron lone pairs and chemical bonds (Fig. 5). The Wannier centre associated with the αCys^{322} S—H bond shifts by 0.01 Å towards the sulphur atom in the presence of αHis^{323}, indicating an increased polar character caused by the π-electron density of the ring and by that of the lone pair of the αHis^{323} Nε. Indeed, the electron density significantly decreases around the thiol H atom (with a net change of about −0.02 e) and correspondingly increases near the thiol S atom (with a net change of about +0.01 e) as a result of the interaction with the imidazole ring (Fig. 5). Thus, the calculations allow us to suggest that the presence of αHis^{323} makes the αCys^{322} S—H bond more polar than usual and hence peculiarly reactive.

The thus established influence of αHis^{323} on the reactivity of αCys^{322} suggests that these two residues could act as a catalytic dyad, with the cysteine in turn influencing the reactivity of the adjacent histidine. The latter has been proposed to act as a base that stabilizes the C-NH_3^+ group that develops following the nucleophilic attack on the urea C atom by the bridging hydroxide and subsequent protonation of the distal urea amide group [8,51]. Based on our density functional theory calculations, we suggest, at the speculative level, that this protonation step could involve the proton shared between these two residues.

An important result of our study is also that we find thiuram disulphides derivatives specifically targeting cysteine residues that form a His-Cys diad. This type of motif is found in several viral cysteine-based proteases and hydrolases, including SARS-CoV-2 M^{pro} and PL^{pro}, even though the efficacy and selectivity are low [69]. Based on the results of the present study, efforts should be directed towards the design of derivatives of thiuram disulphides that are more specific towards urease,

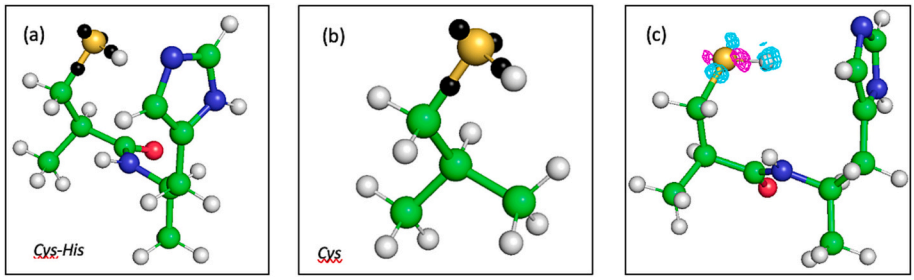

Fig. 5. (a) αCys^{322}-αHis^{323} (*Cys-His*) and (b) αCys^{322} (*Cys*) quantum mechanical models, as obtained after geometry optimization. Colour code: hydrogen (white), carbon (green), sulphur (yellow), nitrogen (blue), oxygen (red). The Wannier centres (black spheres) around the sulphur atom represent the two lone pairs and the two covalent bonds. (c) Difference in electronic density $\Delta\rho = \rho^{Cys\text{-}His}\text{-}\rho^{Cys}$ along the S—H bond. Magenta and cyan regions indicate $\Delta\rho > 0$ (isocontour 0.001 e A^{-3}) and $\Delta\rho < 0$ (isocontour −0.001 e A^{-3}).

possibly including, in the molecule, a functionality able to interact with the Ni(II) ions in the active site. This type of research is ongoing in our laboratory.

Author statement

All authors have contributed equally to the writing of the manuscript.

Declaration of Competing Interest

The authors declare that they have no known competing financial interests or personal relationships that could have appeared to influence the work reported in this paper.

Data availability

Data will be made available on request.

Acknowledgments

The authors acknowledge financial support from the University of Bologna (L.M., A.P., S.C.), the Consorzio Interuniversitario di Risonanze Magnetiche di Metallo-Proteine (CIRMMP) (S.C., L.M.), and the PRIN 2020 “Nature Inspired Crystal Engineering (NICE)”. M.D. acknowledges financial support from the Erasmus+ program of the European Union.

References

[1] M.J. Maroney, S. Ciurli, Chem. Rev. 114 (2014) 4206–4228.
[2] L. Mazzei, F. Musiani, in: S. Ciurli, D. Zamble, M. Rowińska-Żyrek, H. Kozłowski (Eds.), The Biological Chemistry of Nickel, Royal Society of Chemistry, Metallobiology, 2017, pp. 60–97.
[3] A. Evans Journal, 2009.
[4] R.N. Roy, A. Finck, G.J. Blair, H.L.S. Tandon Journal, 2006.
[5] F. Beeckman, H. Motte, T. Beeckman, Curr. Opin. Biotechnol. 50 (2018) 166–173.
[6] D. Mora, S. Arioli, PLoS Pathog. 10 (2014). Public Library of Science. e1004472-e1004472.
[7] L. Mazzei, S. Ciurli, Encycl. Inorg. Bioinorg. Chem, John Wiley & Sons, Ltd, Chichester (UK), 2021, pp. 1–17.
[8] L. Mazzei, F. Musiani, S. Ciurli, J. Biol. Inorg. Chem. 25 (2020) 829–845.
[9] M. Prud'homme, IFA Strategic Forum, Dubai, UAE, 2016.
[10] D. Coskun, D.T. Britto, W. Shi, H.J. Kronzucker, Nature Plants 3, Macmillan Publishers Limited, 2017, p. 17074.
[11] F. Paulot, D.J. Jacob, Environ. Sci. Technol. 48 (2014) 903–908.
[12] X. Zhang, E.A. Davidson, D.L. Mauzerall, T.D. Searchinger, P. Dumas, Y. Shen, Nature 528, Nature Publishing Group, 2015, p. 51, a division of Macmillan Publishers Limited. All Rights Reserved.
[13] X. Zhang, B.B. Ward, D.M. Sigman, Chem. Rev. 120 (2020) 9834.
[14] Y.P. Timilsena, R. Adhikari, P. Casey, T. Muster, H. Gill, B. Adhikari, J. Sci. Food Agric. 95 (2015) 1131–1142.
[15] J.C. Rutherford, PLoS Pathog. 10 (2014) e1004062.
[16] B.M. Roesler, E.M.A. Rabelo-Gonçalves, J.M.R. Zeitune, Clin. Med. Insights Gastroenterol. 7 (2014) 9–17.
[17] I. Konieczna, P. Zarnowiec, M. Kwinkowski, B. Kolesinska, J. Fraczyk, Z. Kaminski, W. Kaca, Curr. Protein Pept. Sci. 13 (2012) 789–806.
[18] B. Marshall, J.R. Warren, Lancet 323 (1984) 1311–1315.
[19] K.A. Eaton, C.L. Brooks, D.R. Morgan, S. Krakowka, Infect. Immun. 59 (1991) 2470–2475.
[20] P. Bauerfeind, R. Garner, B.E. Dunn, H.L.T. Mobley, Gut 40 (1997) 25–30.
[21] K. Stingl, K. Altendorf, E.P. Bakker, Trends Microbiol. 10 (2002) 70–74.
[22] J.G. Kusters, A.H. van Vliet, E.J. Kuipers, Clin. Microbiol. Rev. 19 (2006) 449–490.
[23] J. Baj, A. Forma, M. Sitarz, P. Portincasa, G. Garruti, D. Krasowska, R. Maciejewski, Cells 10 (2020) 27.
[24] C. Zhou, F. Bhinderwala, M.K. Lehman, V.C. Thomas, S.S. Chaudhari, K.J. Yamada, K.W. Foster, R. Powers, T. Kielian, P.D. Fey, PLoS Pathog. 15 (2019) e1007538.
[25] A.H. Gordon, P.D. Hart, M.R. Young, Nature 286 (1980) 79–80.
[26] D.L. Clemens, B.Y. Lee, M.A. Horwitz, J. Bacteriol. 177 (1995) 5644–5652.
[27] W. Lin, V. Mathys, E.L.Y. Ang, V.H.Q. Koh, J.M. Martínez Gómez, M.L.T. Ang, S. Z. Zainul Rahim, M.P. Tan, K. Pethe, S. Alonso, in: J.L. Flynn (Ed.), Infect. Immun 80, 2012, pp. 2771–2779.
[28] R.J. Maier, S.L. Benoit, Inorganics 7 (2019) 80.
[29] WHO, 2017.
[30] WHO, 2022.
[31] L. Casali, L. Mazzei, R. Sun, M.R. Chierotti, R. Gobetto, D. Braga, F. Grepioni, S. Ciurli, Crystal Growth & Design 22, American Chemical Society, 2022, pp. 4528–4537.
[32] E.M. Burnette, S.J. Nieto, E.N. Grodin, L.R. Meredith, B. Hurley, K. Miotto, A. J. Gillis, L.A. Ray, Drugs, 2022.
[33] Y. Lu, Q. Pan, W. Gao, Y. Pu, K. Luo, B. He, Z. Gu, Biomaterials 281 (2022) 121335.
[34] J. Lanz, N. Biniaz-Harris, M. Kuvaldina, S. Jain, K. Lewis, B.A. Fallon, Antibiotics 12 (2023) 524.
[35] N. Fillmore, S. Bell, C. Shen, V. Nguyen, J. La, M. Dubreuil, J. Strymish, M. Brophy, G. Mehta, H. Wu, J. Lieberman, N. Do, C. Sander, PLoS One 16 (2021) e0259061. Public Library of Science.
[36] Á.G. Díaz-Sánchez, A.-P. E., M.-M. A, L. Aguirre-Reyes, O.-O.J.A.M.A. Ramos-Soto, N.-G.J.A.A.-T.B.L.A. de la Rosa, Molecules 21 (2016) 1628–1642.
[37] L. Mazzei, M. Cianci, S. Benini, L. Bertini, F. Musiani, S. Ciurli, J. Inorg. Biochem. 154 (2016) 42–49.
[38] S. Ciurli, C. Marzadori, S. Benini, S. Deiana, C. Gessa, Soil Biol. Biochem. 28 (1996) 811–817.
[39] R.L. Blakeley, E.C. Webb, B. Zerner, Biochemistry 8 (1969) 1984–1990.
[40] B. Krajewska, J. Mol, Catal. B Enzym. 59 (2009) 9–21.
[41] M. Cianci, G. Bourenkov, G. Pompidor, I. Karpics, J. Kallio, I. Bento, M. Roessle, F. Cipriani, S. Fiedler, T.R. Schneider, J. Synchrotron Radiat. 24 (2017) 323–332.
[42] W. Kabsch, Acta Crystallogr. D 66 (2010) 125–132.
[43] P. Evans, Acta Crystallogr. D 62 (2006) 72–82.
[44] P.R. Evans, Acta Crystallogr. D 67 (2011) 282–292.
[45] L. Mazzei, M. Cianci, F. Musiani, G. Lente, M. Palombo, S. Ciurli, J. Inorg. Biochem. 166 (2017) 182–189.
[46] G.N. Murshudov, A.A. Vagin, E.J. Dodson, Acta Crystallogr. D 53 (1997) 240–255.
[47] P. Emsley, K. Cowtan, Acta Crystallogr. D 60 (2004) 2126–2132.
[48] P. Emsley, B. Lohkamp, W.G. Scott, K. Cowtan, Acta Crystallogr. D 66 (2010) 486–501.
[49] M.J. Abraham, T. Murtola, R. Schulz, S. Páll, J.C. Smith, B. Hess, E. Lindahl, SoftwareX 1-2 (2015) 19–25.
[50] S. Páll, M.J. Abraham, C. Kutzner, B. Hess, E. Lindahl, Proc. Solving Software Challenges for Exascale 3-27, Springer International Publishing, Cham, 2015.
[51] L. Mazzei, M. Cianci, S. Benini, S. Ciurli, Angew. Chem. Int. Ed. Eng. 58 (2019) 7415–7419.
[52] L. Mazzei, M. Cianci, S. Benini, S. Ciurli, Chem. Eur. J. 25 (2019) 12145–12158.
[53] J. Hutter, A. Alavi, T. Deutsch, M. Bernasconi, S. Goedecker, D. Marx, M. Tuckerman, M. Parrinello, MPI für Festkörperforschung Stuttgart, 1990-2022.
[54] A.D. Becke, J. Chem. Phys. 97 (1992) 9173–9177.
[55] G.J. Martyna, M.E. Tuckerman, J. Chem. Phys. 110 (1999) 2810–2821.
[56] N. Troullier, J.L. Martins, Phys. Rev. B 43 (1992) 1993–2006.
[57] N. Marzari, D. Vanderbilt, Phys. Rev. B 56 (1997) 12847.
[58] P.L. Silvestrelli, N. Marzari, D. Vanderbilt, P. M, Solid State Commun. 107 (1998) 7–11.
[59] R. Capelli, W. Liu, V. Bolnykh, S. Meloni, J.M.H. Olsen, U. Rothlisberger, M. Parrinello, P. Carloni, J. Phys. Chem. Lett. 11 (2020) 6373–6381.

[60] S. Benini, M. Cianci, L. Mazzei, S. Ciurli, J. Biol. Inorg. Chem. 19 (2014) 1243–1261.
[61] M.J. Todd, R.P. Hausinger, J. Biol. Chem. 266 (1991) 10260–10267.
[62] M.J. Todd, R.P. Hausinger, J. Biol. Chem. 266 (1991) 24327–24331.
[63] S. Benini, W.R. Rypniewski, K.S. Wilson, S. Ciurli, S. Mangani, J. Biol. Inorg. Chem. 3 (1998) 268–273.
[64] L. Mazzei, M. Cianci, A. Gonzalez Vara, S. Ciurli, Dalton Trans. 47 (2018) 8240–8247.
[65] L. Mazzei, D. Cirri, M. Cianci, L. Messori, S. Ciurli, J. Inorg. Biochem. 218 (2021) 111375.
[66] L. Mazzei, U. Contaldo, F. Musiani, M. Cianci, G. Bagnolini, M. Roberti, S. Ciurli, Angew. Chem. Int. Ed. Eng. 60 (2021) 6029–6035.
[67] K. Macegoniuk, W. Tabor, L. Mazzei, M. Cianci, M. Giurg, K. Olech, M. Burda-Grabowska, R. Kaleta, A. Grabowiecka, A. Mucha, S. Ciurli, L. Berlicki, J. Med. Chem. 66 (2023) 2054–2063.
[68] I.-S. Park, R.P. Hausinger, Protein Sci. 2 (1993) 1034–1041.
[69] C. Ma, Y. Hu, J.A. Townsend, P.I. Lagarias, M.T. Marty, A. Kolocouris, J. Wang, ACS Pharmacology & Translational Science 3, American Chemical Society, 2020, pp. 1265–1277.
[70] M.D. Winn, C.C. Ballard, K.D. Cowtan, E.J. Dodson, P. Emsley, P.R. Evans, R. M. Keegan, E.B. Krissinel, A.G. Leslie, A. McCoy, S.J. McNicholas, G.N. Murshudov, N.S. Pannu, E.A. Potterton, H.R. Powell, R.J. Read, A. Vagin, K.S. Wilson, Acta Crystallogr. D 67 (2011) 235–242.
[71] D.W. Cruickshank, Acta Crystallogr. D 55 (1999) 583–601.
[72] E.F. Pettersen, T.D. Goddard, C.C. Huang, G.S. Couch, D.M. Greenblatt, E.C. Meng, T.E. Ferrin, J. Comput. Chem. 25 (2004) 1605–1612.